Chemosphere 289 (2022) 133233

Contents lists available at ScienceDirect

Chemosphere

journal homepage: www.elsevier.com/locate/chemosphere

# Toxic effects of $SiO_2$NPs in early embryogenesis of *Xenopus laevis*

Rosa Carotenuto [a,*,1], Margherita Tussellino [a,1], Raffaele Ronca [b], Giovanna Benvenuto [c], Chiara Fogliano [a], Sabato Fusco [d], Paolo Antonio Netti [e,f,g]

[a] Department of Biology, University of Naples Federico II, Naples, Italy
[b] Institute of Biostructures and Bioimaging (IBB)-CNR, Naples, Italy
[c] Stazione Zoologica "Anton Dohrn" Naples, Italy
[d] Department of Medicine and Health Sciences "Vincenzo Tiberio", University of Molise, Campobasso, Italy
[e] Center for Advanced Biomaterials for Health Care (CABHC), Italian Institute of Technology, Naples, Italy
[f] Interdisciplinary Research Centre on Biomaterials (CRIB), University of Naples Federico II, Naples, Italy
[g] Department of Chemical Materials and Industrial Production (DICMAPI), University of Naples Federico II, Naples, Italy

## HIGHLIGHTS

- The effects of $SiO_2$NPs was evaluated for early development of *Xenopus laevis*.
- The concentration/effect relationship is not linear.
- $SiO_2$NPs modify the expression of genes implied in *Xenopus laevis* development.
- $SiO_2$NPs induce ROS production in *Xenopus laevis* embryos.

## GRAPHICAL ABSTRACT

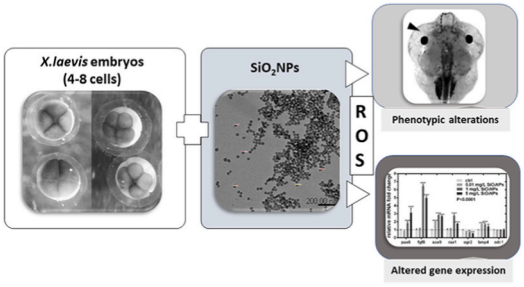


## ARTICLE INFO

Handling Editor: Willie Peijnenburg

*Keywords:*
Embryogenesis
*X. laevis*
$SiO_2$NPs
Gene expression
Toxicity
ROS

## ABSTRACT

The exposure of organisms to the nanoparticulate is potentially hazardous, particularly when it occurs during embryogenesis. The effects of commercial $SiO_2$NPs in early development were studied, using *Xenopus laevis* as a model to investigate their possible future employment by means of the Frog Embryo Teratogenesis Assay-*Xenopus* test (FETAX). The $SiO_2$NPs did not change the survival but produced several abnormalities in developing embryos, in particular, the dorsal pigmentation, the cartilages of the head and branchial arches were modified; the encephalon, spinal cord and nerves are anomalous and the intestinal brush border show signs of suffering; these embryos are also bradycardic. In addition, the expression of genes involved in the early pathways of embryo development was modified. Treated embryos showed an increase of reactive oxygen species. This study suggests that $SiO_2$NPs are toxic but non-lethal and showed potential teratogenic effects in *Xenopus*. The latter may be due to their cellular accumulation and/or to the effect caused by the interaction of $SiO_2$NPs with cytoplasmic and/or nuclear components. ROS production could contribute to the observed effects. In conclusion, the data indicates that the use of $SiO_2$NPs requires close attention and further studies to better clarify their activity in animals, including humans.

* Corresponding author. Department of Biology, University of Naples, Via Cinthia, Ed. 7, 80126, Naples, Italy.
*E-mail address:* rosa.carotenuto@unina.it (R. Carotenuto).
[1] Rosa Carotenuto and Margherita Tussellino contribute equally to the work.

https://doi.org/10.1016/j.chemosphere.2021.133233
Received 8 September 2021; Received in revised form 6 December 2021; Accepted 7 December 2021
Available online 8 December 2021

## 1. Introduction

Nanoparticles are included in many consumer products to improve the handling, stability, and efficacy of these products. Their unique properties are also exploited in therapeutic drug delivery and imaging techniques; therefore, it appears that the general population is constantly exposed to nanoparticles. The aquatic environment is particularly at risk of exposure to nanoparticles (NPs) as it acts as a sink for most environmental contaminants (Tussellino et al., 2015; Libralato et al., 2017; Duan et al., 2013b). Whilst data indicates that, in general, some nanoparticles are potentially harmful to exposed aquatic organisms, sufficient evidence is lacking for almost all NPs considered. More standardized approaches are required for NPs hazard identification and interaction occurring between nanomaterials and living systems (Tussellino et al., 2015; Galdiero et al., 2017; Libralato et al., 2017). $SiO_2$ is the most abundant compound in the Earth's crust and could, in the form of nanoparticles, bioaccumulate in the environment and along the food chain with possible hazardous effects (Napierska et al., 2010). Among various types of nanoparticles, the silica nanoparticles ($SiO_2$NPs), are considered stable and non-toxic and are favored as nanostructuring, drug delivery, and optical imaging agents (Formosa et al., 2015; Saint-Cricq et al., 2015; Sonin et al., 2016). They are also applied in the remediation of the environment pollutants (see Jeelani et al., 2020), used as an additive for the manufacturing of rubber and plastics, as strengthening filler for concrete and other construction composites, as anti-caking agent to maintain flow properties in powdered products and as a carrier for fragrances or flavors in food and nonfood products (Robberecht et al., 2008; Dekkers et al., 2011; Martirosyan and Schneider, 2014). Furthermore, as generally considered non-toxic for humans, $SiO_2$NPs have been added to food products for some years and have been registered with the EU as a food additive (E551) (Athinarayanan et al., 2014; van Kesteren et al., 2015). It is estimated that over one million tons of $SiO_2$NPs are used annually in consumer products (Jarvie et al., 2009a) and much of that is believed to get washed down the drains into the aquatic milieu (Jarvie et al., 2009b), data on environmental concentrations of $SiO_2$NPs is lacking, including data relating concentrations in the vicinity of industrial areas or densely populated areas. (Book and Backhaus, 2021). For the reasons indicated above, it could be predicted that in the near future silica NPs may be accumulated by animals, including humans and cause damage. Indeed, previous studies on $SiO_2$NPs in human and mammalian generally showed that, both *in vivo* and *in vitro*, their toxicity was dose-, time-, and size-dependent with high doses, longer exposures, and smaller particles being most toxic (Napierska et al., 2009, 2010; De Matteis, 2017; Chen et al., 2018; Maynard et al., 2011). Conflicting results indicated that $SiO_2$NPs may accumulate in the mammalian liver, lung, and spleen tissue and potentially damage their functions (Xie et al., 2010). Exposure to $SiO_2$NPs increased levels of reactive oxygen species and antioxidant enzymes (Eom and Choi, 2009; Ramesh et al., 2013), decreased glutathione levels and lipid peroxidation resulting in beyond-threshold oxidative stress (Yang et al., 2009; Ahamed, 2013; PetracheVoicu et al., 2015). In fact, it was found that mitochondrial damage leading to oxidative stress and apoptosis was the direct cause of cytotoxicity by $SiO_2$NPs in human hepatoma HepG2 cells (Sun et al., 2011). Exposure to the silica nanoparticles has dramatic effects on *D. melanogaster* development as midgut cells of exposed larvae undergo membrane destabilization with increased cell death after internalization of $SiO_2$NPs (Pandey et al., 2013). However, the effects of $SiO_2$NPs on aquatic biota, in particular amphibian, were not extensively studied and require further studies.

The aim of this study is to understand the effects that uncoated $SiO_2$NPs have on the embryogenesis of the well-known model *Xenopus laevis*, for the assessment of their effect on aquatic larvae thus contributing to the understanding of their possible toxicity and subsequent harm for this amphibian and general aquatic community. *Xenopus* is a valuable model in the study of pathways involved in development or of factors inducing cancer (Lobikin et al., 2012; Hardwick and Philpott, 2015). Moreover, due to the close homology of its genome with the human genome (Tomlinson et al., 2005: Takagi et al., 2013; Session et al., 2016; Tandon et al., 2017) *Xenopus* offers the important possibility to transfer and apply the data obtained to higher vertebrates including humans. Furthermore, the fact that experiments on *X. laevis* can usually be undertaken in a short time and at small expense allows a large number of tests and subjects to be carried out and analyzed. *X. laevis* development takes place outside the mother's body in simple salt solutions, therefore allowing an easy screening of embryonic morphogenesis. Tadpoles are transparent, facilitating the detection of tissue and organ defects (Bonfanti et al., 2020). The literature regarding *Xenopus*, that deal with the potential effect of $SiO_2$ nanoparticles are not available, apart from Ozmen et al. (2018) who affirm that the synthesized $SiO_2$NPs had no toxic effect on *X. laevis* and *D. rerio* embryos.

In this paper, commercial $SiO_2$ nanoparticles were used as a model to understand the possible consequences deriving from the use of similar NPs, utilized in both medicine and food, to investigate the suitability of their uses in the future. The modified FETAX protocol was applied, consequently endpoints such as: survival, malformations, growth, pigment distribution and heart rate in *Xenopus laevis* development (Tussellino et al., 2015; Mouche et al., 2017; Fort and Mathis, 2018) were analyzed. During vertebrate embryogenesis, a correct regulation of gene expression is crucial for proper body plan determination. As it can be questioned whether $SiO_2$NPs are able to act directly or indirectly on gene expression, Real-Time PCR was used to investigate possible alterations caused by $SiO_2$NPs, where the expression of some genes governing the pathways essential for normal embryonic development were investigated. For this reason, a group of genes that could provide the first indications concerning the observed phenotypic modifications were chosen. Therefore, the expression of genes involved in the axis formation were studied such as fgf8, that is involved in embryo posteriorization and bmp4, that is mainly involved in embryo ventralization (Hongo et al.,1999; Heasman, 2006; Hong, 2008; Reich and Weinstein, 2019); pax6 and rax1 related to eye development (Hirsch and Harris, 1997; Giudetti et al., 2014); sox9 and egr2 essential for neural crest formation (sox9) and migration (egr2) in *Xenopus* (Spokony et al., 2002; Lee et al., 2004; Stuhlmiller, 2012; Tussellino et al., 2016). Finally, the production of reactive oxygen species (ROS) was studied to understand if the observed effects could depend on their increased production.

## 2. Materials and methods

### 2.1. Animals

Adult *Xenopus laevis* were obtained from Nasco (Fort Atkinsons, Wisconsin, USA). They were kept and used at the Department of Biology of the University of Naples, Federico II, according to the guidelines and policies dictated by the University Animal Welfare Office in agreement with international rules and in strict accordance with the recommendations in the Guide for the Care and Use of Laboratory Animals of the National Institutes of Health of the Italian Ministry of Health. The protocol was approved by the Committee on the Ethics of Animal Experiments (Centro Servizi Veterinari) of the University of Naples Federico II (Permit Number: 2014/0017970). All procedures were performed according to Italian ministerial authorization (DL 116/92) and European regulations on the protection of animals employed for experimental and other scientific purposes. All treatments were adopted in line with these regulations to minimize suffering. To obtain eggs, *X. laevis* females were injected in the dorsal lymphatic sac with 500 units of Gonase (AMSA) in amphibian Ringer solution (111 mM NaCl, 1.3 mM $CaCl_2$, 2 mM KCl, 0.8 mM $MgSO_4$, in 25 mM Hepes, pH7.8). Fertilized eggs and embryos were obtained by standard insemination methods (Tussellino et al., 2015) and staged according to Nieuwkoop and Faber (1956).

### 2.2. $SiO_2$NPs characterization

$SiO_2$NPs were purchased from MKnano-Canada (Mississauga-Ontario): MKN-$SiO_2$-S020 Silica Spherical Nanoparticles in Aqueous media, Concentration: 5%, Size 20 nm (Customs Code: 2850.0000). The size of the NPs fell within the range of sizes that easily penetrate cells (Nam et al., 2013) and nucleus (Symens et al., 2011).

Dynamic light scattering (DLS), performed with a Zetasizer Nano-ZS (Malvern Instruments, Worcestershire, UK), was carried out to measure $SiO_2$NPs size and z-potential. Measures were conducted at 21 °C, using $SiO_2$NPs diluted to 1 mg/L in $H_2O$, the medium used by the manufacturer in amphibian solution (FETAX: pH7.4 106 mM NaCl, 11 mM $NaHCO_3$, 4 mM KCl, 1 mM $CaCl_2$, 4 mM $CaSO_4$, 3 mM $MgSO_4$). Measures were performed in triplicate. The effective NPs diameters and their size distributions were measured by transmission electron microscopy (TEM). Formvar-coated 200 mesh copper grids were used and the excess of water or FETAX was gently blotted using filter paper. Dried grids were directly inserted into a Jeol-JEM1220 transmission electron microscope (Jeol, Akishima, Tokyo) operating at 100 kV and images were collected at a magnification of ×50,000 using a dedicated CCD. 100 NPs were measured, and the median, mean and standard deviation were calculated.

### 2.3. $SiO_2$NPs exposition

FETAX assay was modified, by anticipating the contact of the embryos with the NPs at St. 4/8 cells, to study the gene expression of early embryonic development; furthermore this adaption was because it was closer to natural conditions, where embryos are exposed to NPs earlier than the original FETAX test.

Stages 4/8 cells embryos were placed and grown in FETAX solution containing $SiO_2$NPs at the following concentrations: 0.01 mg/L, 1 mg/L or 5 mg/L. The range of concentration used to test these NPs in *Xenopus* and other organisms were selected (Casado et al., 2013; Duan et al., 2013b; Lajmanovich et al., 2018; Ozmen et al., 2018; and EFSA Panel, 2018). The modified FETAX assay was used to test single compounds as in Tussellino et al. (2015), where embryos were collected and dejelled with 0.3% β-mercaptoethanol (pH 9.0) for 1/2 min. Embryos at stage 4/8, that had been normally cleaved were selected for testing and placed in 10.0 cm, glass Petri dish, with 15 embryos per dish which each contained 50 mL of either control or test solution. Sibling embryos were used as a control group. All embryos were raised and exposed up to stage 45/46, at which time the survivors were collected (Nieuwkoop and Faber, 1956). For each experimental group, the dead embryos were recorded and removed daily. The experiments were carried out at 21 °C, under a 12 h light: 12 h dark photoperiod. The pH (7.4) of the solutions in the Petri dishes containing the embryos was checked every day. For each female subject, the test was replicated 3 times for the control group and for each of the compound concentration groups. Two females were used in each test and at least three tests were performed. The surviving embryos were anaesthetized with MS-222 (Sigma-Aldrich) at a concentration of 100 mg/L and evaluated for every single malformation by examining each specimen under a stereo microscope Leica MZ16F UV stereomicroscope (Leica Microsystems s.r.l., Milan Italy), integrated with LED Ring Light, equipped with a Leica DFC 300Fx camera and IM50 Image Manager Software.

### 2.4. Phenotype analysis

Phenotype analysis was carried out at stage 45/46, five days after the beginning of the treatment, with a Leica MZ16F UV stereomicroscope (Leica Microsystems s.r.l., Milan Italy), integrated with LED Ring Light, equipped with a Leica DFC 300Fx camera and IM50 Image Manager Software.

After anesthesia in FETAX with 100 mg/L MS-222 (SIGMA), a photo of each tadpole was taken in the ventral position, to check the morphology of the intestinal area, and in the dorsal position to determine its length and pigmentation. Length determination of embryos was assessed via the embryo photos with the software Adobe Photoshop CS5 (Adobe Systems Software Ireland Ltd., Dublin, Ireland), calibrating length via a ruler photographed at the same magnification as the tadpoles. The pigment of the dorsal area, between the region of the olfactory bulbs and the spinal cord was also quantified via two graphic programs: Adobe Photoshop CS5 (in order to highlight and calculate the degree of basic dorsal pigmentation and to standardize the collected images) and Image-ProPlus 6.0 (Media Cybernetics, Inc., Rockville, MD, USA), to determine the percentage of pigment present in the relevant anatomic cut out by analysing the percentage of image pixels with the same grey level. The tadpoles' heart rate measurement (expressed in beats per minute) was performed using a dissection microscope (Wild, Heerbrugg), through recording the number of heartbeats for 30 s, three times. For each type of analysis performed, data obtained was normalized by dividing each treated embryo measure by the average value of the control tadpoles (Tussellino et al., 2016; Carotenuto et al., 2016).

### 2.5. Electron microscopy

Since the treated embryos presented growth problems, the intestine (as it is responsible for the absorption of nutrients) was investigated for damage. Control and exposed embryos were randomly selected and, after anesthesia, fixed in 2.5% glutaraldehyde for 18 h at 4 °C, before ultrastructural analysis. They were then washed three times in 0.1 M sodium cacodylate, embedded in 3% low melting agarose, post-fixed with 1% osmium tetroxide at 4 °C for 1hr, rinsed five times with 0.1 M sodium cacodylate buffer, dehydrated in a graded ethanol series, further substituted by propylene oxide and embedded in Epon 812 (TAAB, TAAB Laboratories Equipment Ltd, Berkshire, UK) at room temperature for 1 day and polymerized at 60 °C for 2 days. Resin blocks were sectioned with an Ultracut UCT ultramicrotome (Leica, Wetzlar, Germany). 70 nm ultrathin sections were placed on nickel grids, contrasted with 4% aqueous uranyl acetate for 30 min s, rinsed once with a mix of methanol and bi-distilled water (1:1), twice with bi-distilled water and observed with a Zeiss LEO 196 912AB EFTEM (Zeiss, Oberkochen, Germany).

### 2.6. Whole-mount immunolocalization

Having observed malformations affecting the nervous system derivatives, the extent was then verified using the acetylated tubulin as a marker, which is important for the regulation of many processes associated with the maturation and function of neurons. Control and exposed *X. laevis* embryos, after anesthesia, were fixed in MEMFA (MOPS (4-morpholinepropanesulfonic acid), EGTA, $MgSO_4$, Formaldehyde) (100 mM MOPS pH7.4, 2 mM EGTA, 1 mM $MgSO_4$, 3.7% v/v Formaldehyde) (see Gont et al., 1993) at stage 45/46 and stored in 100% ethanol at −20 °C. Embryos were incubated with monoclonal anti-tubulin acetylated (SIGMA, T6793, which is specifically reactive to amphibians also) diluted 1:100 in PBS containing 0.5% BSA and 0.1% Triton X100 for 24 h at 4 °C. The antibody excess was eliminated via washes in PBS for 24 h at 4 °C. Embryos were subsequently incubated with goat anti-mouse IgG BODIPY conjugated (Molecular Probes, B-2752) diluted 1:200 for 24 h at 4 °C. All samples were photographed with a Leica MZ16F UV stereomicroscope, equipped with a Leica DFC 300Fx camera and IM50 Image Manager Software (Tussellino et al., 2016).

### 2.7. Real-time PCR analysis

Target gene mRNA was quantified with quantitative real-time PCR. All analyses were carried out using the Applied Biosystem 7500 Real-Time PCR System and the Power SYBR®Green PCR Master Mix (Life Technologies) in 20 μl total reaction volume, following procedures recommended by the manufacturer. cDNA was synthesized using

SuperScript R VILO cDNA synthesis kits (Life Technologies) and 2 μg of total RNA. Used primers are indicated in Table 3. The amplification thermal profile is as follows: 95 °C for 3 min (initial DNA denaturation); 40 cycles of 95 °C for 15 s and 60 °C for 1min. A final dissociation curve assay was performed for each reaction to confirm gene-specific amplification (see Carotenuto et al., 2020).

### 2.8. Oxygen reactive species analysis

The intracellular ROS were determined according to Eliso et al. (2020). Control and $SiO_2$NPs exposed embryos (St. 45/46) were rinsed twice with FETAX and incubated with 10 mM of fluorescent dye 2′, 7′–dichlorodihydrofluorescin diacetate (DCFH-DA, Sigma-Aldrich), at RT for 2hrs in dark conditions. Control samples were incubated with DMSO. After incubation, embryos were rinsed twice with FETAX, resuspended in 0.5 mL of 40 mM Tris–HCl buffer (pH 7) homogenated and then centrifuged (13000 rpm) for 10 min s at 4 °C; supernatant was used for the fluorescence measurement at an excitation wavelength of 488 nm and an emission wavelength of 525 nm using a spectrofluorometer (Synergy H4 microplate reader, Biotek). Fluorescence values were normalized by subtracting the autofluorescence from unlabeled extracts (DMSO). Results were expressed as arbitrary units of fluorescence referred to 36 embryos'.

### 2.9. Statistical analysis

Statistical tests to compare untreated and control groups were conducted for all experiments with the Graph Pad Prism 6 software (San Diego, California USA).

The percentage of survival embryos and all malformations were compared using the Chi square test and Yate's correction for continuity or using the Fisher's Exact test. The survival distributions in control and experimental groups were also assessed in terms of significance using nonparametric Mantel-Cox test. Differences in heartrate, length and dorsal pigmentation of the embryos were examined by ANOVA with non-parametric Kruskal–Wallis test and Dunn's test for *post-hoc* analysis. Real time data analysis was performed using Two-way Anova with Bonferroni's test. ROS activities were analyzed using a One-Way ANOVA followed by Bonferroni's *post hoc* Test. The analysis was performed three times.

## 3. Results

### 3.1. $SiO_2$NPs characterization

$SiO_2$NPs were characterised with TEM microscopy and DLS. Electron microscopy showed that in both water and FETAX, the $SiO_2$NPs were found to be mildly electron-dense (Fig. 1A and B) have a spherical shape (Fig. 1 B) and have an average diameter of 30 nm (Fig. 1B and C).

The z-potential was measured to elucidate the colloidal stability of nanoparticles. The colloidal stability of NPs in suspension is strongly pH-dependent, mainly due to electrostatic repulsion. Table 1 shows that the $SiO_2$NPs z-potential, measured within 1 h of dilution in $H_2O$ or in FETAX, ranged from circa −9 to −12 mVs respectively, values allowing particle aggregation. It should be remembered that, according to current literature (Tussellino et al., 2015), $SiO_2$NPs may aggregate at z-potential values between ±30 mV. Indeed, in FETAX the z-average indicates the presence of aggregates of about 180 nm and in water at about 60 nm. The Polydispersity Index (PdI) (>0.2) indicated that they were unevenly distributed (Table 1).

### 3.2. $SiO_2$NPs do not cause embryonic death

The embryos raised from St. 4/8 cells up to St. 45/46 in the presence of $SiO_2$NPs (n = 569), with a concentration of 0.01, 1 and 5 mg/L, showed a percentage of survival between 87.56% and 82.14% (n = 490), (Fig. 2A and Table 2).

### 3.3. $SiO_2$NPs modify growth rate and phenotype of the treated embryos

Significant nonlinear concentration-dependent modifications of growth ($p < 0.0001$) was observed in treated embryos. In fact, the embryos showed a modified length compared to the control (Fig. 2B). In particular, embryos treated with 0.01 and 1 mg/L $SiO_2$NPs showed a

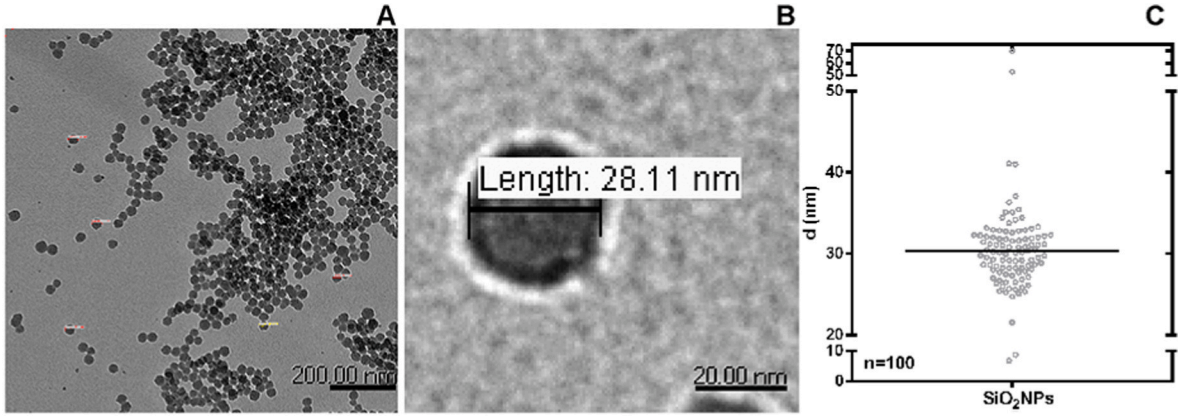


**Fig. 1.** Nanoparticle's characterization.
A-B transmission electron microscopy. A = 20000×, B magnification of image A (ten fold). C. Size distribution of nanomaterials: median 30.12 nm, mean 30.36 nm and standard deviation 6.445.

**Table 1**
Dynamic light scattering of $SiO_2$NPs in $H_2O$ and FETAX solution.

| | Size [nm] | Size [SD] | Z-potential [mV] | Z-potential [SD] | PdI | PdI [SD] |
|---|---|---|---|---|---|---|
| $H_2O$ | 63,83 ± 4,087[a] | 12,26 | −9183 ± 1,006[a] | 3019 | 0,3896 ± 0,02034[a] | 0,06101 |
| FETAX | 184,9 ± 47,85[a] | 143,6 | −12,59 ± 3,503[a] | 10,51 | 0,6703 ± 0,1072[a] | 0,3216 |

[a] ) [a] Mean value ± SE, n = 3; SD= Standard Deviation.

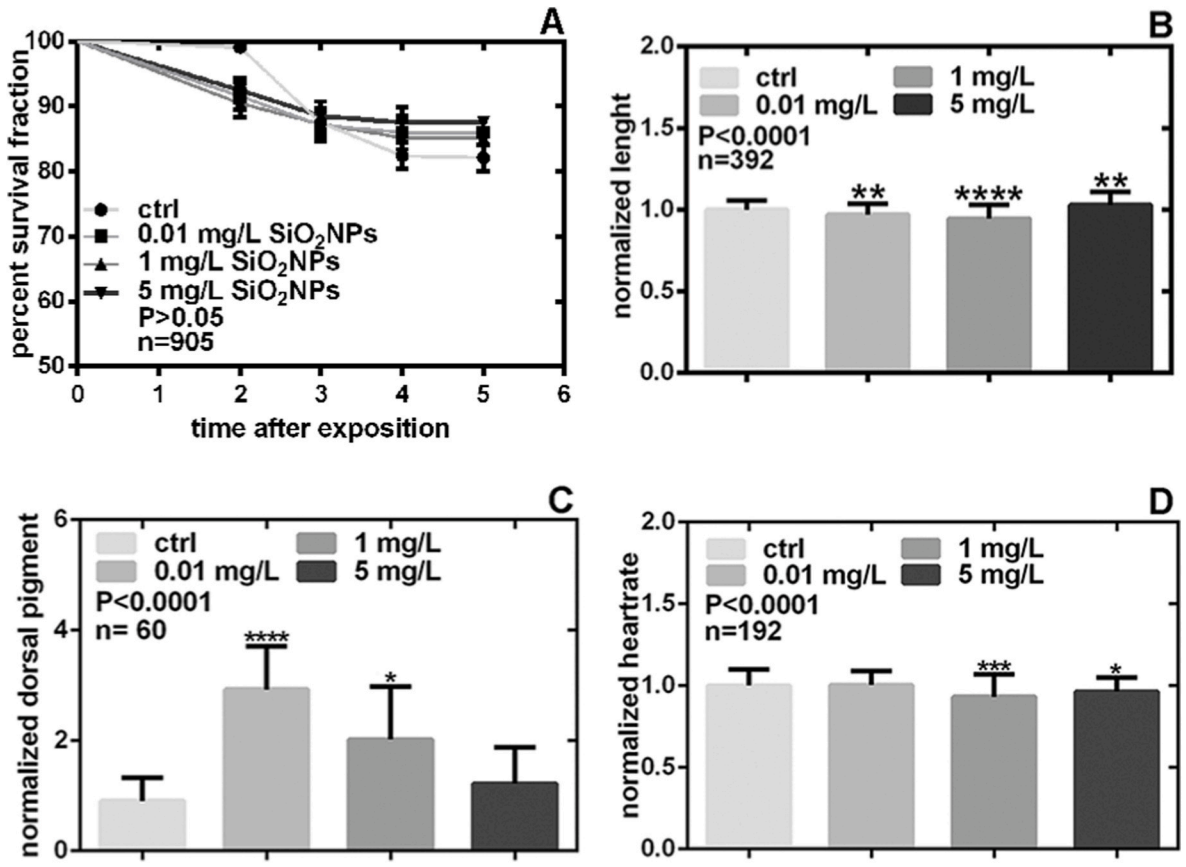


**Fig. 2.** Survival and phenotypic evaluation of embryos raised in $SiO_2$NPs.
The survival distribution was evaluated by non-parametric Mantel-Cox test giving P > 0.05 ($SiO_2$NPs treatment with 0.01 mg/L compared to control, $p = 0.2468$; 1 mg/L compared to control, $p = 0.7767$; 5 mg/L compared to control, $p = 0.4281$). The experimental points represent the average of three independent experiments. The error bars indicate the standard error. In B, C and D. Evaluation of length, dorsal pigment and heartrate analysis in embryos (mean and standard deviation). In B for each group (control or treated) were used 98 embryos. In C were used 15 embryos for each group. In D were used 48 embryos for control and for all single treatment. All data were analyzed by ANOVA with non-parametric Kruskal–Wallis test and Dunn's test for *post-hoc* analysis. *$p < 0.05$; **$p < 0.01$; ***$p < 0.001$; ****$p <$ 0,0001.

**Table 2**
*Xenopus laevis* embryos survival.

| | utilized (n) | dead (n) | living (n) | survival fraction (%) |
|---|---|---|---|---|
| Untreated | 336 | 60 [a] | 276[a] | 82.14 |
| 0.01 mg/L | 180 | 25 [a] | 155 [a] | 86.11 |
| 1 mg/L | 188 | 29 [a] | 159 [a] | 84.57 |
| 5 mg/L | 201 | 25 [a] | 176 [a] | 87.56 |

n = number embryos used; [a] Chi square test; P > 0.05.

length corresponding to stage 42/43, when sibling embryos attained stage 45/46 (Fig. 2B and data not shown). In contrast, 5 mg/L treated embryos were longer than the control subjects.

Like other toxicants, $SiO_2$NPs produced a number of malformations in developing embryos (Figs. 2–5) concerning derivatives of all three germ layers: ectoderm, endoderm and mesoderm. These malformations are visible at all concentrations but seen more clearly higher frequency at 0.01 and 1 mg/L. Fig. 2C describes dorsal pigment distribution in five-day-old embryos. Embryos treated at 0,01 mg/L $SiO_2$NPs showed a greater concentration of pigment compared to control groups. The pigment concentration decreased as the concentration of NPs increased. Epidermal melanocytes result randomly distributed and often clustered along the dorsal area of the skin covering the encephalon (compare control in Fig. 3A with treated embryos Fig. 3A'). In some embryos NPs clustered around the eyes where they show a characteristic accumulation (Fig. 3B, arrows). Moreover, a modified pigment distribution was observed in the retina "pigmented layer", that appears partially depigmented (Fig. 3B', arrowhead). In treated embryos, magnification of melanocytes show that the pigment fills the entire cytoplasm (Fig. 3 D-D′, white circle), in contrast to control embryos where the pigment

**Table 3**
Primers.

| Gene name | Oligo Forward Sequence | Oligo Reverse Sequence | Accession Number |
|---|---|---|---|
| bmp4 - bone morphogenetic protein 4 | CCTCAGCAGCATTCCAGAGAA | TCCGGTGGAAACCCTCATCC | NM_001101793 |
| egr2 - early growth response 2 | AGTAAGACCCCAGTCCACGA | GCAGTAATCGCAGGCAAAGG | NM_001085779.1 |
| fgf8 - fibroblast growth factor 8 | CGTTTGGAAGCAGAGTTCGC | GTTGCCTTGTCTTCGACCCT | NM_001090435.1 |
| odc1 - ornithine decarboxylase | GTGGCAAGGAATCACCCGAA | TCAAAGACACATCGTGCATC | NM_001086698.1 |
| pax6 - paired box protein Pax-6 | CAGAACATCTTTTACCCAGGA | GAATGTGGCTGGGTGTGTTA | NM_001172195.2 |
| rax1 - retinal homeobox protein Rx1 | GGAAAGACCTCAAGCGAGTG | ATACCTGCACCCTGACCTCG | NM_001088218.1 |
| sox9 - sex determining region Y-box 9 | ACGGCGCAGAAAGTCTGTTA | GACATCTGTCTTGGGGGTGG | NM_001090807.1 |

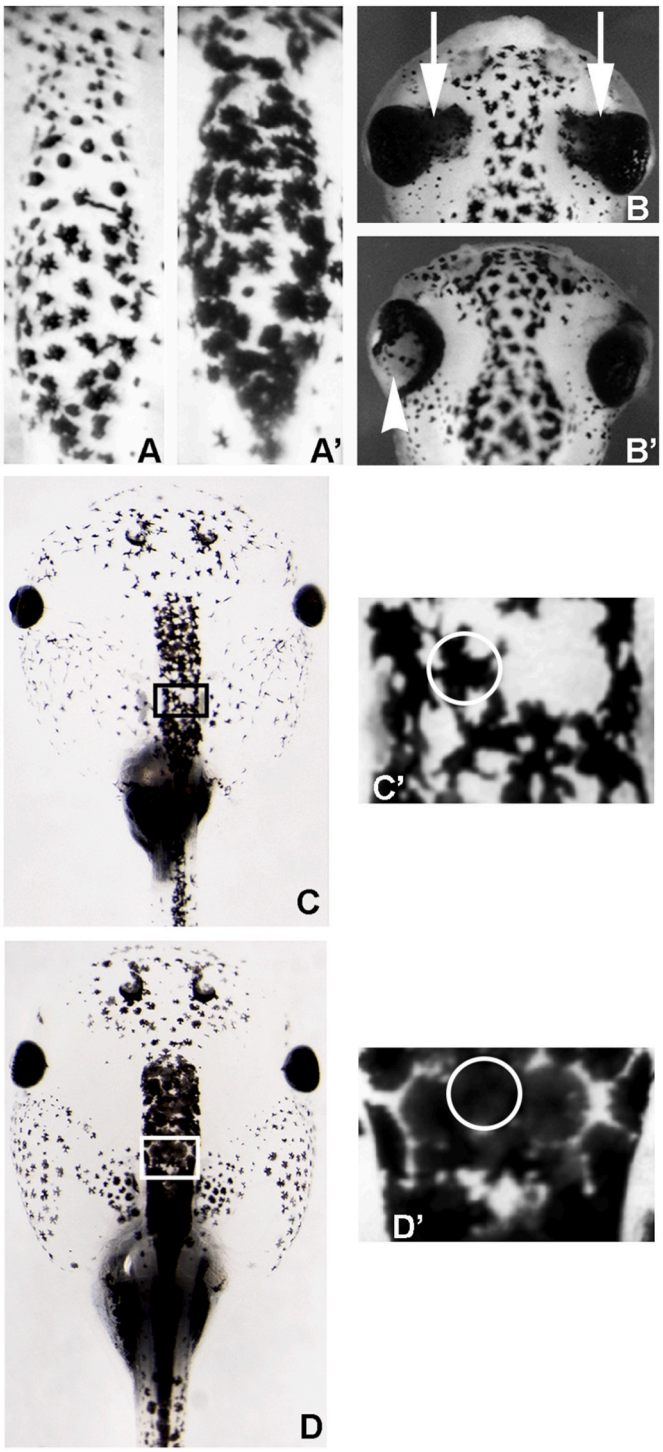


**Fig. 3.** Dorsal pigment distribution of tadpoles raised in $SiO_2$NPs.
All embryos are in dorsal view. A-A'. Skin covering encephalon in control embryo (A) and treated embryo (A′). B-B'. The abnormal pigment distribution in treated embryos around the eyes. The withe arrows indicate excess pigmentation, the head-arrow the zone without pigment. C-C'. The dorsal area of control tadpole (C) and its magnification (C′) compared to the same area of the treated embryos (D-D′). In C′ and D' white circles indicate single cells.

appears to be star-shaped and is not distributed throughout the cytoplasm (Fig. 3 C-C', white circle).

Embryos show abnormalities in the winding of the intestine that appears immature (Fig. 4 B-C, arrow) compared to sibling controls (Fig. 4 A) and stopped their development at stage 42(B) or 43(C) (see Chalmers and Slack, 1998, to compare intestinal winding) in a percentage of 13–36% (data not shown). The severity of problems in the intestines, which is responsible for the absorption of nutrients, was tested for damage. Histological screening with electron microscopy showed that in treated embryos the digestive system and, in particular, the small intestine was affected (Fig. 4D–G). In fact, the brush border exhibits areas without microvilli (E, arrowhead, and compare with the controls, D), with shorter microvilli (F, arrowhead) or fused microvilli (G, asterisk). The exposed embryos also showed head malformations (Fig. 5A', B′ and D′) and a widespread edema (Fig. 5 B′, arrowhead). Cartilages of facial skeleton were compressed (Fig. 5 A′, arrows), and in particular the Meckel cartilage (Fig. 5 B′, dotted line) that protrudes from the skull. Also, the gill basket appears smaller than in control subjects (Fig. 5C and C′, dotted line) and the gills, that in the control embryos are transparent, appear opaque in treated embryos probably due to an NPs obstruction (Fig. 5 C-C′, double arrows). Some embryos displayed problems related to the morphology of the encephalon and the spinal cord. In general, all the encephalic vesicles showed abnormalities and are not clearly distinguishable. (Fig. 5 D-D′, dashed line). Indeed, immunofluorescence data showed that the olfactory bulbs are indistinguishable from the forebrain (Fig. 5 D-D′ asterisk) that appears deformed and the hindbrain larger than in control embryos (Fig. 5 D-D′, arrow). In some cases, the complete absence of an eye (Fig. 5 D-D′, arrowhead) was verified. Moreover, the spinal cord is very thin (Fig. 5 D-D′, double arrows) and the cranial nerves are barely detectable (Fig. 5 D-D').

### 3.4. Heartrate modification

Treated embryos showed modification of the heartrate; they are, in fact, bradycardic compared to control groups, in particular those embryos treated with 1 mg/L $SiO_2$NPs (Fig. 2 D).

### 3.5. $SiO_2$NPS produce alteration of genes expression

Based on the abnormalities observed in treated embryos, the possible alterations of gene expression caused by $SiO_2$NPs were explored in early *X. laevis* development. Real Time-PCR, conducted on surviving embryos harvested at St. 45/46, showed a general modification of gene expression in treated embryos (Fig. 6). In particular, at 0.01 mg/L nanoparticle concentration, the gene expression of treated embryos is similar to the expression of the controls with the exception of sox9 and bmp4 that were overexpressed and egr2 that appeared downregulated. In contrast, at 1 and 5 mg/L $SiO_2$NPs concentration, the genes are mildly overexpressed, with the exception of egr2 that is downregulated, and fgf8 that is between 5 and 7 times more expressed than in control subjects.

#### 3.5.1. Reactive oxygen species

The results of the DCF-DA assay in *X. laevis* embryos (St. 45/46) exposed to $SiO_2$NPs (0.01, 1; 5 mg/L) are shown in Fig. 7. A dose-dependent increase in fluorescence was observed with significant higher values at 1 and 5 mg/L compared to control groups.

## 4. Discussion

The aim of this study was to test the toxic potential of $SiO_2$ nanoparticles on the development of *X. laevis*. The studies were conducted using the modified FETAX protocol as in Tussellino et al. (2015). TEM data indicates an effective size of 30 nm on average of these NPs while DLS showed presence of aggregates; Hackley and Clogston (2015) discuss the possibility that the differences in size of the NPs verified by DLS and TEM are due to the different principles inspiring the two techniques.

The FETAX data indicates that, within the range of studied concentrations, the $SiO_2$NPs do not modify survival rate of the exposed embryos compared to the control groups but cause some modifications to the

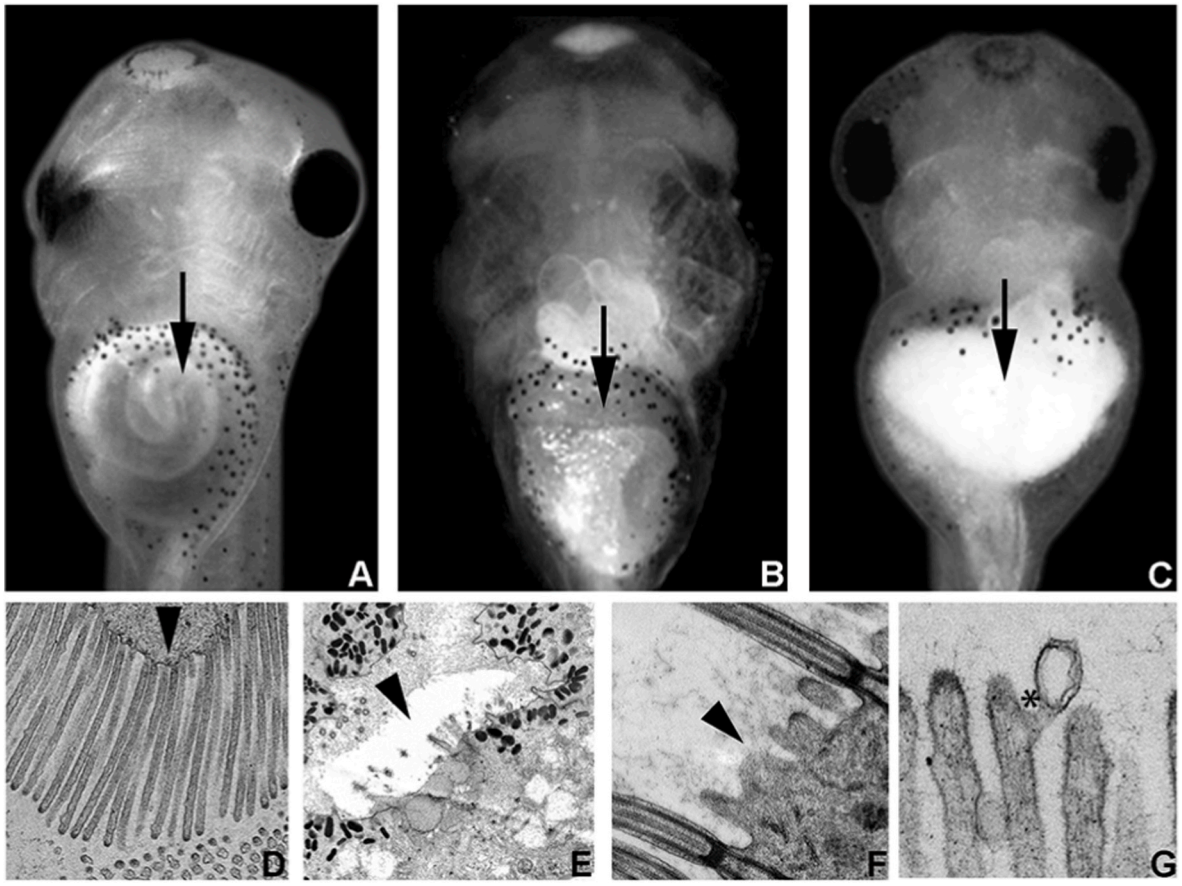


**Fig. 4.** Gut modification in treated embryos.
All embryos were in ventral view. A. Control embryo (St. 45/46). B. Treated embryo showing an immature gut, St. 43, compared to control embryo (A). C. Treated embryo showing an immature gut, St. 42, compared to control embryo (A). The black arrow point to gut. D-G. Histological sections of intestinal brush border in control (D) and treated embryos (E-G) observed with TEM. The arrowhead show microvilli conditions and asterisk microvilli fusion. Magnification: 10000×.

phenotype. Ozmen et al. (2018) showed that synthesized fluorescent $SiO_2$NPs have no significant toxic effect on *X. laevis* embryos, and that photocatalytic degradation of the dye fluorescence significantly reduced the observed effects on embryonic stages of this organism. In zebrafish, Xue et al. (2013) proved that $SiO_2$NPs of 15 and 50 nm caused mortality according to size and concentration and Vranic et al. (2019) showed that $SiO_2$NPs of 25 and 115 nm significantly reduced the survival of zebrafish dechorionated embryos. Our data indicated that $SiO_2$NPs influence embryonic growth at all concentrations but with varying effects. The observed biphasic trend in embryonic growth could suggest a hormetic effect. However, hormesis correlates with stimulatory responses at low doses and inhibitory responses at high doses and our data indicates a stimulatory action at high doses of Nps (5 mg/L). It could be hypothesized that the formation of aggregates at the highest concentration greatly reduces the entry of NPs, this could cause the observed effects. In *Xenopus,* have been proved that nanoparticles and toxicants are involved in the modification of embryonic stages progression (Nations et al., 2010, 2015; Tussellino et al., 2015, 2016). Gibeaux et al. (2018) showed that *Xenopus* transcriptional regulation controls the size of tailbuds, suggesting that differential gene expression contributes to size differences of embryos. It has been suggested that both hes7,due to the role it plays in the segmentation of somites, (Bessho et al., 2003) and genes participating in the generation and maintenance of the dorso-ventral embryonic gradient of BMP4 signalling (Lee et al., 2002) have a role in the development of the size of embryos. In zebrafish embryos, $SiO_2$NPs impair somitogenesis by weakening physiological Wnt signalling (Yi et al., 2016). This study showed $SiO_2$NPs induce a modification of expression of bmp4 and fgf8 in *Xenopus* embryos. In particular, Real Time PCR indicated that fgf8 was very highly expressed while bmp4 was only slightly upregulated. In Xenopus, wnt and fgf/bmp signalling pathways play important roles in regulating the patterning of embryo axes (Itoh and Sokol, 1999; Yamaguchi, 2001; Heasman, 2006; Lou et al., 2006; Dorey and Amaya, 2010). Further data is needed to learn the expression pattern of these genes thus allowing a possible correlation with an irregular A/P axis formation.

The extent of intestinal winding, a parameter that together with the body length helps the identification of the embryonic stages, was also modified (Chalmers and Slack, 1998). Treated embryos had an intestinal winding that was comparable to younger-stage embryos. It should be considered that Bmp4 plays a major role in the specification, regionalization and differentiation in the developing gut (Smith et al., 2000) by acting on FoxF1 (Mahlapuu et al., 2001; Tseng et al., 2004). These may correlate with the abnormal coiling seen in the gut of the treated embryos, where bmp4 expression was modified.

At lower concentrations, previous data related to the length of the embryo and intestine winding correlate, indicating that the embryos reached a younger stage than the control group. In contrast, when treated at 5 mg/L, treated embryos were longer, although showing a more immature intestine compared to the control group, this could be dependent on the modification of the expression of bmp4 and fgf8 shown by the treated embryos.

Moreover, it can be speculated that at the highest concentration of $SiO_2$NPs used, the formation of aggregates is greater and therefore the quantity of NPs that can enter the embryo decreases, this being sufficient to impair the correct intestine formation, yet not enough to slow the embryonic growth (Nations et al., 2015). Furthermore, the extending of

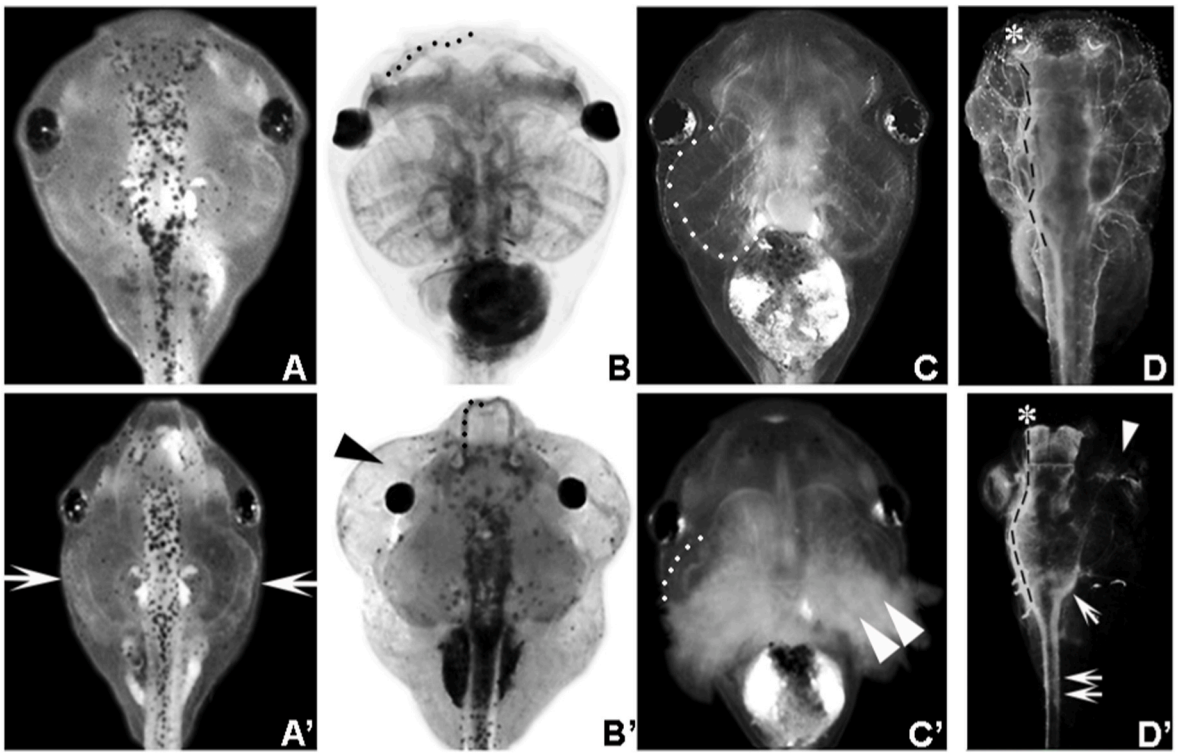


**Fig. 5.** $SiO_2$NPs treated embryos malformations.
A-D. Untreated embryos. A′-D′ treated embryos. A'. The head was compressed (arrows). B'. The Meckel's cartilage protruded (black dotted line) and there were edema (black arrowhead). C'. Gill basket was smaller (white dotted line) and gills were opaque (double arrows-head). D'. Encephalon alterations: olfactory bulbs (asterisk), missing eye (white arrowhead), swollen hindbrain (arrow), thinned spinal cord (double arrows). The fragmented line in D and D′ indicate the border of the encephalon.

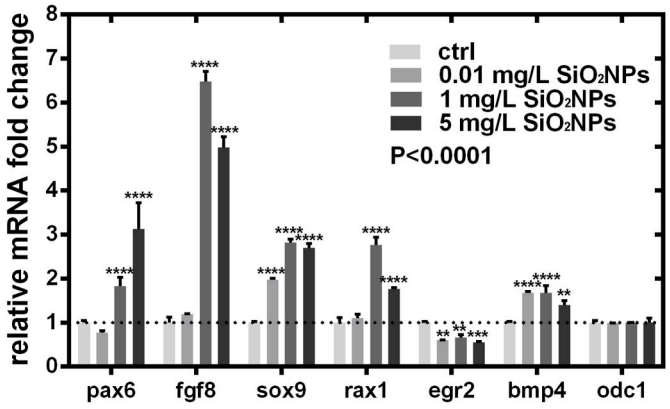


**Fig. 6.** Real-Time PCR analysis of genes involved in early development.
Data are presented as mean with SD. Statistical significance was determined usingOne-Way ANOVA followed by Bonferroni's *post hoc* Test. $^{*}p < 0.05$, $^{**}p < 0.01$, $^{***}p < 0.001$ and $^{****}p < 0.0001$.

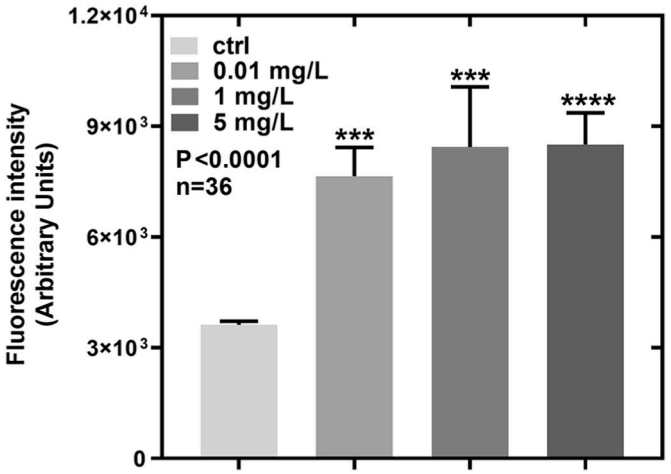


**Fig. 7.** Reactive oxygen species production.
Quantitative analyses of intracellular ROS levels (fluorescence arbitrary units) of *X. laevis* embryos (St. 45/46) exposed to $SiO_2$NPs (0.01, 1, 5 mg/L). Bars represent mean ± SD (n = 36). Asterisks indicate values that are significantly different compared to the controls (One-Way ANOVA followed by Bonferroni's *post hoc* test) $^{***}p < 0.001$, $^{****}p < 0.0001$.

the growth time could be attributed to a modification of the metabolism which, at lower concentrations of $SiO_2$NPs, may lead to the observed slowdown in growth (Nations et al., 2015). Finally, TEM microscopy showed suffering of the intestinal brush border that showed areas without microvilli or with altered morphology. The brush border is essential for the absorption of nutrients and therefore for the growth and wellness of the embryos. It must be considered that starting from stage 39/40, the embryos open their mouths and the NPs ingested reaching the intestine, where they can exert their negative effects. Alterations of the intestine by $SiO_2$NPs have also been found in other organisms such as zebrafish (Bai and Tang, 2020) and *D. melanogaster* where they have dramatic effects on midgut cells (Pandey et al., 2013).

An irregular position of the pigmented skin cells were also observed. Melanocytes stem from the neural crest, the transient multipotent cells deriving by delamination from the developing neural tube (Le Douarin and Creuzet, 2011). In *Xenopus*, formation, delamination, and final differentiation of these migrating cells (Cheung and Briscoe, 2003; Lee et al., 2004) depend upon sox9 and egr2 transcripts, downstream of fgf

and a bmp4/wnt1 expression gradient (Adameyko et al., 2009; Martínez-Morales et al., 2011; Theveneau and Mayor, 2012; Tussellino et al., 2016; Ji et al., 2019). In treated embryos an overexpression of bmp4 and sox9 was observed while egr2 was noted as downregulated. This anomalous expression could explain the increased number of melanocytes and their anomalous distribution which in vertebrates also derive from egr2 transcripts (Adameyko et al., 2009). The mechanism by which the NPs alter melanocyte distribution in the head is unclear. However, it can be inferred that exposure to $SiO_2$NPs affects cell cycle progression and/or cell proliferation in the dorsal area, without affecting their primary differentiation. Moreover, our results indicate that melanocytes have an anomalous distribution of internal pigment. The latter could depend upon "mechanical stress'' produced by the amount of nanoparticles penetrated into the melanocytes and interfering with the movement of melanosomes along the microtubules within the cells (see Barral and Seabra, 2004; Jiang et al., 2020).

Treated embryos also showed an extensive edema that compressed the internal organs causing difficulties in organ activity, as seen in the heart that resulted bradycardic, particularly at 1 mg/L. In zebrafish silica nanoparticles caused bradycardia (Duan et al., 2013a). Yet, it cannot be omitted that the observed modified expressions of fgf8, bmp4 and sox9 contributed to this phenotype, as these genes are required for the development of the cardiovascular system (Reifers et al., 2000; Shi et al., 2000; Abu-Issa et al., 2002; Alsan and Schultheiss, 2002; van Wijk et al., 2007; Gawdzik et al., 2018). In addition, serious anomalies concerning the cartilage skeleton deriving from the first 2 branchial arches of the splanchnocranium were described. Different cranial neural crest-derived structures and gill basket resulted compressed, and the rostral portion of Meckel's cartilage protruded from the skull. This could be due to the edema, but also due to the alteration of the expression of genes involved in the specification and movement of the neural crests. During neurulation, cranial NCC delaminate and migrate to areas of the head, where they condense to form cartilage elements of the branchial arches and ventral skull (Mancilla and Mayor, 1996; Le Douarin et al., 2007). In $SiO_2$NPs exposed embryos, these structures were correctly located, suggesting that the NCC migration pathway was not affected despite the observed, slight downregulation of egr2. The observed defects may depend on altered genetic signalling involved in cartilage formation. The data indicates that $SiO_2$NPs had a direct effect on genes such as fgf8, bmp4, sox9 and egr2, genes that are essential for the outgrowth of maxillary and fronto-nasal skeletal elements (Schneider et al., 2001; Mina et al., 2002; Santagati and Rijli, 2003). We detected phenotypes showing deformations of the fore- and hindbrain, eyes, olfactive bulbs, cranial nerves, and spinal cord thinning. The observed malformations could be explained by considering the Real Time PCR data which showed modifications of the expression of genes essential for a correct development of the anterior/posterior neural axis (fgf/bmp) and of master genes involved in the development of the eye as pax6 and rax1 (Casarosa et al., 1997; Gehring and Ikeo, 1999; Ohkubo et al., 2002; Manuel and Price, 2005), but also of the sox9 and egr2 involved in cranial nerves formation and myelination (Topilko et al., 1997).

The Real Time PCR data stimulated hypothesis that $SiO_2$NPs which were used, could enter the nucleus (Symens et al., 2011) and act directly on the genome (Pogribna and Hammons, 2021). Gong et al. (2012) showed that, in Ha-CaTcells, $SiO_2$NPs induced decrease of PARP-1 mRNA expression by methylation of PARP-1 promoter. In human BEAS-2B cells, exposure to silica nanoparticles caused DNA hypermethylation of CREB3L1 and Bcl-2 which is associated with apoptosis (Zou et al., 2016). The observed modification of gene expression could be due to the increase in ROS production, the findings of this study also show that $SiO_2$NPs provoke the production of ROS at both low and high concentrations in treated *Xenopus* embryos. Indeed, it is well known that nanoparticles have a high tendency to generate excessive amounts of reactive oxygen species that result in high damage to cells, including DNA/RNA breakage or even mutagenesis (Yu et al., 2020).

## 5. Conclusions

The present study showed that silica nanoparticles, which are considered stable and non-toxic, showed a toxic/teratogenic effect in *X. laevis* embryogenesis. The study showed no linear relationship between the $SiO_2$NPs concentration and observed effects. This may be due to the amount of NPs that penetrate the cells and then to their cellular accumulation and/or to the effects caused by the interaction of $SiO_2$NPs with cytoplasmic components or via penetration of the nucleus where they act directly on the genome. ROS could be the cause of observed effects. In conclusion, our data indicates that the use of $SiO_2$NPs requires high attention and further studies to better clarify their activity in animals, including humans.

## Credit author statement

Carotenuto Rosa: Project administration, Resources, Supervision, Data curation, Writing – original draft. Tussellino Margherita: Conceptualization, Methodology, Formal analysis, Reviewing and Editing, Validation. Ronca Raffaele: Methodology, Validation. Benvenuto Giovanna: Methodology. Fogliano Chiara: Methodology, Formal analysis. Fusco Sabato: Validation. Netti Paolo: Conceptualization.Supervision.

## Declaration of competing interest

The authors declare that they have no known competing financial interests or personal relationships that could have appeared to influence the work reported in this paper.

## Acknowledgement

This research did not receive any specific grant from funding agencies in the public, commercial, or not-for-profit sectors.

We are grateful to Prof.ssa Chiara Campanella for her support.

## References

Abu-Issa, R., Smyth, G., Smoak, I., Yamamura, K., Meyers, E.N., 2002. Fgf8 is required for pharyngeal arch and cardiovascular development in the mouse. Development (Camb. Engl.) 129 (19), 4613–4625.

Adameyko, I., Lallemend, F., Aquino, J.B., Pereira, J.A., Topilko, P., Müller, T., Fritz, N., Beljajeva, A., Mochii, M., Liste, I., Usoskin, D., Suter, U., Birchmeier, C., Ernfors, P., 2009. Schwann cell precursors from nerve innervation are a cellular origin of melanocytes in skin. Cell 139 (2), 366–379.

Ahamed, M., 2013. Silica nanoparticles-induced cytotoxicity, oxidative stress and apoptosis in cultured A431 and A549 cells. Hum. Exp. Toxicol. 32 (2), 186–195.

Alsan, B.H., Schultheiss, T.M., 2002. Regulation of avian cardiogenesis by Fgf8 signaling. Development (Camb. Engl.) 129 (8), 1935–1943.

Athinarayanan, J., Periasamy, V.S., Alsaif, M.A., Al-Warthan, A.A., Alshatwi, A.A., 2014. Presence of nanosilica (E551) in commercial food products: TNF-mediated oxidative stress and altered cell cycle progression in human lung fibroblast cells. Cell Biol. Toxicol. 30 (2), 89–100.

Bai, C., Tang, M., 2020. Toxicological study of metal and metal oxide nanoparticles in zebrafish. J. Appl. Toxicol. 40 (1), 37–63.

Barral, D.C., Seabra, M.C., 2004. The melanosome as a model to study organelle motility in mammals. Pigm. Cell Res. 17 (2), 111–118.

Bessho, Y., Hirata, H., Masamizu, Y., Kageyama, R., 2003. Periodicrepression by the bHLHfactor Hes7 is an essentialmechanism for the somitesegmentation clock. Genes Dev. 17, 1451–1456.

Bonfanti, P., Colombo, A., Saibene, M., Fiandra, L., Armenia, I., Gamberoni, F., Gornati, R., Bernardini, G., Mantecca, P., 2020. Iron nanoparticle bio-interactions evaluated in Xenopus laevis embryos, a model for studying the safety of ingested nanoparticles. Nanotoxicology 14 (2), 196–213.

Book, F., Backhaus, T., 2021. Aquatic ecotoxicity of manufactured silica nanoparticles: a systematic review and meta-analysis. Sci. Total Environ., 150893 (Advance online publication).

Carotenuto, R., Tussellino, M., Mettivier, G., Russo, P., 2016. Survival fraction and phenotype alterations of Xenopus laevis embryos at 3 Gy, 150 kV X-ray irradiation. Biochem. Biophys. Res. Commun. 480 (2016), 580–585.

Carotenuto, R., Capriello, T., Cofone, R., Galdiero, G., Fogliano, C., Ferrandino, I., 2020. Impact of copper in Xenopus laevis liver: histological damages and atp7b downregulation. Ecotoxicol. Environ. Saf. 188, 109940.

Casado, M.P., Macken, A., Byrne, H.J., 2013. Ecotoxicological assessment of silica and polystyrene nanoparticles assessed by a multitrophic test battery. Environ. Int. 51, 97–105.

Casarosa, S., Andreazzoli, M., Simeone, A., Barsacchi, G., 1997. Xrx1, a novel Xenopus homeobox gene expressed during eye and pineal gland development. Mech. Develop. 61 (1–2), 187–198. https://doi.org/10.1016/s0925-4773(96)00640-5.
Chalmers, A.D., Slack, J.M., 1998. Development of the gut in Xenopuslaevis. Dev. Dynam. 212 (4), 509–521.
Chen, L., Liu, J., Zhang, Y., Zhang, G., Kang, Y., Chen, A., Feng, X., Shao, L., 2018. The toxicity of silica nanoparticles to the immune system. Nanomedicine 13 (15), 1939–1962.
Cheung, M., Briscoe, J., 2003. Neural crest development is regulated by the transcription factor Sox9. Development 130 (23), 5681–5693.
De Matteis, V., 2017. Exposure to inorganic nanoparticles: routes of entry, immune response, biodistribution and in vitro/in vivo toxicity evaluation. Toxics 5 (4), 29.
Dekkers, S., Krystek, P., Peters, R.J., Lankveld, D.P., Bokkers, B.G., van Hoeven-Arentzen, P.H., Bouwmeester, H., Oomen, A.G., 2011. Presence and risks of nanosilica in food products. Nanotoxicology 5 (3), 393–405.
Dorey, K., Amaya, E., 2010. FGF signalling: diverse roles during early vertebrate embryogenesis. Development (Camb. Engl.) 137 (22), 3731–3742.
Duan, J., Yu, Y., Li, Y., Yu, Y., Sun, Z., 2013a. Cardiovascular toxicity evaluation of silica nanoparticles in endothelial cells and zebrafish model. Biomaterials 34 (23), 5853–5862.
Duan, J., Yu, Y., Shi, H., Tian, L., Guo, C., Huang, P., Zhou, X., Peng, S., Sun, Z., 2013b. Toxic effects of silica nanoparticles on zebrafish embryos and larvae. PLoS One 8 (9), e74606.
EFSA ANS Panel (EFSA Panel on Food Additives and Nutrient Sources added to Food), Younes, M., Aggett, P., Aguilar, F., Crebelli, R., Dusemund, B., Filipič, M., Frutos, M. J., Galtier, P., Gott, D., Gundert-Remy, U., Kuhnle, G.G., Leblanc, J.-C., Lillegaard, I. T., Moldeus, P., Mortensen, A., Oskarsson, A., Stankovic, I., Waalkens-Berendsen, I., Woutersen, R.A., Wright, M., Boon, P., Chrysafidis, D., Gürtler, R., Mosesso, P., Parent-Massin, D., Tobback, P., Kovalkovicova, N., Rincon, A.M., Tard, A., Lambré, C., 2018. Scientific Opinion on the re-evaluation of silicon dioxide (E 551) as a food additive. EFSA J. 16 (1), 5088.
Eliso, M.C., Bergami, E., Manfra, L., Spagnuolo, A., Corsi, I., 2020. Toxicity of nanoplastics during the embryogenesis of the ascidian Ciona robusta (Phylum Chordata). Nanotoxicology 14 (10), 1415–1431.
Eom, H.J., Choi, J., 2009. Oxidative stress of silica nanoparticles in human bronchial epithelial cell, Beas-2B. Toxicol. Vitro 23 (7), 1326–1332.
Formosa, C., Schiavone, M., Boisrame, A., Richard, M.L., Duval, R.E., Dague, E., 2015. Multiparametric imaging of adhesive nanodomains at the surface of Candida albicans by atomic force microscopy. Nanomedicine 11 (1), 57–65.
Fort, D.J., Mathis, M., 2018. Frog embryo Teratogenesis assay-Xenopus (FETAX): use in alternative preclinical safety assessment. Cold Spring Harb. Protoc. 2018 (8).
Galdiero, E., Falanga, A., Siciliano, A., Maselli, V., Guida, M., Carotenuto, R., Tussellino, M., Lombardi, L., Benvenuto, G., Galdiero, S., 2017. *Daphnia magna* and *Xenopus laevis* as in vivo models to probe toxicity and uptake of quantum dots functionalized with gH625. Int. J. Nanomed. 12, 2717–2731.
Gawdzik, J.C., Yue, M.S., Martin, N.R., Elemans, L.M.H., Lanham, K.A., Heideman, W., Rezendes, R., Baker, T.R., Taylor, M.R., Plavicki, J.S., 2018. Sox9b is required in cardiomyocytes for cardiac morphogenesis and function. Sci. Rep. 8 (1), 13906.
Gehring, W.J., Ikeo, K., 1999. Pax 6: mastering eye morphogenesis and eye evolution. Trends Genet.: TIG (Trends Genet.) 15 (9), 371–377.
Gibeaux, R., Acker, R., Kitaoka, M., Georgiou, G., van Kruijsbergen, I., Ford, B., Marcotte, E.M., Nomura, D.K., Kwon, T., Veenstra, G., Heald, R., 2018. Paternal chromosome loss and metabolic crisis contribute to hybrid inviability in Xenopus. Nature 553 (7688), 337–341.
Giudetti, G., Giannaccini, M., Biasci, D., Mariotti, S., Degl'innocenti, A., Perrotta, M., Barsacchi, G., Andreazzoli, M., 2014. Characterization of the Rx1-dependent transcriptome during early retinal development. Dev. Dynam. 243 (10), 1352–1361.
Gong, C., Tao, G., Yang, L., Liu, J., Liu, Q., Li, W., Zhuang, Z., 2012. Methylation of PARP-1 promoter involved in the regulation of nano-SiO2-induced decrease of PARP-1 mRNA expression. Toxicol. Lett. 209 (3), 264–269.
Gont, L.K., Steinbeisser, H., Blumberg, B., deRobertis, E.M., 1993. Tail formation as a continuation of gastrulation: the multiple cell populations of the Xenopus tailbud derive from the late blastopore lip. Development (Camb. Engl.) 119 (4), 991–1004.
Hackley, V., Clogston, J., 2015. Measuring the Size of Nanoparticles in Aqueous Media Using Batch-Mode Dynamic Light Scattering, Special Publication (NIST SP 1200-6). National Institute of Standards and Technology, Gaithersburg, MD.
Hardwick, L.J., Philpott, A., 2015. An oncologist's friend: how Xenopus contributes to cancer research. Dev. Biol. 408 (2), 180–187.
Heasman, J., 2006. Patterning the early Xenopus embryo. Development (Camb. Engl.) 133 (7), 1205–1217.
Hirsch, N., Harris, W.A., 1997. Xenopus Pax-6 and retinal development. J. Neurobiol. 32 (1), 45–61.
Hong, C.S., Park, B.Y., Saint-Jeannet, J.P., 2008. Fgf8a induces neural crest indirectly through the activation of Wnt8 in the paraxial mesoderm. Development (Camb. Engl.) 135 (23), 3903–3910.
Hongo, I., Kengaku, M., Okamoto, H., 1999. FGF signaling and the anterior neural induction in Xenopus. Dev. Biol. 216 (2), 561–581.
Itoh, K., Sokol, S.Y., 1999. Axis determination by inhibition of Wnt signaling in Xenopus. Genes Dev. 13 (17), 2328–2336.
Jarvie, H.P., Al-Obaidi, H., King, S.M., Bowes, M.J., Lawrence, M.J., Drake, A.F., Green, M.A., Dobson, P.J., 2009a. Managing Nanoparticle Waste in Sewage. ISIS Science and Technology Facilities Council. http://www.isis.stfc.ac.uk/science/earth-science-and-environment/managing-nanoparticle-waste-in-sewage9094.html.
Jarvie, H.P., Al-Obaidi, H., King, S.M., Bowes, M.J., Lawrence, M.J., Drake, A.F., Green, M.A., Dobson, P.J., 2009b. Fate of silica nanoparticles in simulated primary wastewater treatment. Environ. Sci. Technol. 43 (22), 8622–8628.
Jeelani, P.G., Mulay, P., Venkat, R., Ramalingam, C., 2020. Multifaceted application of silica nanoparticles. A Review. Silicon 12, 1337–1354.
Ji, Y., Hao, H., Reynolds, K., McMahon, M., Zhou, C.J., 2019. Wnt signaling in neural crest ontogenesis and oncogenesis. Cells 8 (10), 1173.
Jiang, M., Paniagua, A.E., Volland, S., Wang, H., Balaji, A., Li, D.G., Lopes, V.S., Burgess, B.L., Williams, D.S., 2020. Microtubule motor transport in the delivery of melanosomes to the actin-rich apical domain of the retinal pigment epithelium. J. Cell Sci. 133 (15), jcs242214.
Lajmanovich, R.C., Peltzer, P.M., Martinuzzi, C.S., Attademo, A.M., Colussi, C.L., Basso, A., 2018. Acute toxicity of colloidal silicon dioxide nanoparticles on Amphibian larvae: emerging environmental concern. Int. J. Environ. Res. 12, 269–278.
Le Douarin, N.M., Brito, J.M., Creuzet, S., 2007. Role of the neural crest in face and brain development. Brain Res. Rev. 55 (2), 237–247.
Le Douarin, N.M., Creuzet, S., 2011. Crête neurale et évolution des vertébrés [Neural crest and vertebrate evolution]. Biologie aujourd'hui 205 (2), 87–94.
Lee, H.S., Park, M.J., Lee, S.Y., Hwang, Y.S., Lee, H., Roh, D.H., Kim, J.I., Park, J.B., Lee, J.Y., Kung, H.F., Kim, J., 2002. Transcriptional regulation of Xbr-1a/Xvent-2 homeobox gene: analysis of its promoter region. Biochem. Biophys. Res. Commun. 298 (5), 815–823.
Lee, Y.H., Aoki, Y., Hong, C.S., Saint-Germain, N., Credidio, C., Saint-Jeannet, J.P., 2004. Early requirement of the transcriptional activator Sox9 for neural crest specification in Xenopus. Dev. Biol. 275 (1), 93–103.
Libralato, G., Galdiero, E., Falanga, A., Carotenuto, R., De Alteriis, E., Guida, M., 2017. Toxicity effects of functionalized quantum dots, gold and polystyrene nanoparticles on target aquatic biological models: a review. Molecules 22, 1439.
Lobikin, M., Chernet, B., Lobo, D., Levin, M., 2012. Resting potential, oncogene-induced tumorigenesis, and metastasis: the bioelectric basis of cancer in vivo. Phys. Biol. 9 (6), 065002.
Lou, X., Fang, P., Li, S., Hu, R.Y., Kuerner, K.M., Steinbeisser, H., Ding, X., 2006. Xenopus Tbx6 mediates posterior patterning via activation of Wnt and FGF signalling. Cell Res. 16 (9), 771–779.
Mahlapuu, M., Enerbäck, S., Carlsson, P., 2001. Haploinsufficiency of the forkhead gene Foxf1, a target for sonic hedgehog signaling, causes lung and foregut malformations. Development 128 (12), 2397–2406.
Mancilla, A., Mayor, R., 1996. Neural crest formation in Xenopus laevis: mechanisms of Xslug induction. Dev. Biol. 177 (2), 580–589.
Manuel, M., Price, D.J., 2005. Role of Pax6 in forebrain regionalization. Brain Res. Bull. 66 (4–6), 387–393.
Martínez-Morales, P.L., Diez del Corral, R., Olivera-Martínez, I., Quiroga, A.C., Das, R.M., Barbas, J.A., Storey, K.G., Morales, A.V., 2011. FGF and retinoic acid activity gradients control the timing of neural crest cell emigration in the trunk. J. Cell Biol. 194 (3), 489–503.
Martirosyan, A., Schneider, Y.J., 2014. Engineered nanomaterials in food: implications for food safety and consumer health. Int. J. Environ. Res. Publ. Health 11 (6), 5720–5750.
Maynard, A.D., Warheit, D.B., Philbert, M.A., 2011. The new toxicology of sophisticated materials: nanotoxicology and beyond. Toxicol. Sci. 120 (Suppl. 1), S109–S129.
Mina, M., Wang, Y.H., Ivanisevic, A.M., Upholt, W.B., Rodgers, B., 2002. Region- and stage-specific effects of FGFs and BMPs in chick mandibular morphogenesis. Dev. Dynam. 223 (3), 333–352.
Mouche, I., Malésic, L., Gillardeaux, O., 2017. FETAX assay for evaluation of developmental toxicity. Methods Mol. Biol. 1641, 311–324.
Nam, J., Won, N., Bang, J., Jin, H., Park, J., Jung, S., Jung, S., Park, Y., Kim, S., 2013. Surface engineering of inorganic nanoparticles for imaging and therapy. Adv. Drug Deliv. Rev. 65 (5), 622–648.
Napierska, D., Thomassen, L.C., Lison, D., Martens, J.A., Hoet, P.H., 2010. The nanosilica hazard: another variable entity. Part. Fibre Toxicol. 7 (1), 39.
Napierska, D., Thomassen, L.C., Rabolli, V., Lison, D., Gonzalez, L., Kirsch-Volders, M., Martens, J.A., Hoet, P.H., 2009. Size-dependent cytotoxicity of monodisperse silica nanoparticles in human endothelial cells. Small 5 (7), 846–853.
Nations, S., Long, M., Wages, M., Maul, J.D., Theodorakis, C.W., Cobb, G.P., 2015. Subchronic and chronic developmental effects of copper oxide (CuO) nanoparticles on *Xenopuslaevis*. Chemosphere 135, 166–174.
Nations, S., Long, M., Wages, M., Theodorakis, C., Cobb, G.P., 2010. Developmental effects of ZnO nanoparticle on Xenopus laevis. Ecotoxicol. Environ. Saf. 74, 203–210.
Nieuwkoop, P.D., Faber, J., 1956. Normal Table of Xenopus laevis (Daudin): A Systematical and Chronologica Survey of the Development from the Fertilized Egg till the End of Metamorphosis. North-Holland, Amsterdam.
Ohkubo, Y., Chiang, C., Rubenstein, J.L., 2002. Coordinate regulation and synergistic actions of BMP4, SHH and FGF8 in the rostral prosencephalon regulate morphogenesis of the telencephalic and optic vesicles. Neuroscience 111 (1), 1–17.
Ozmen, N., Erdemoglu, S., Gungordu, A., Asilturk, M., Turhan, D.O., Akgeyik, E., Harper, S.L., Ozmen, M., 2018. Photocatalytic degradation of azo dye using core@shell nano-TiO2 particles to reduce toxicity. Environ. Sci. Pollut. Res. 25, 29493–29504.
Pandey, A., Chandra, S., Chauhan, L.K., Narayan, G., Chowdhuri, D.K., 2013. Cellular internalization and stress response of ingested amorphous silica nanoparticles in the midgut of Drosophila melanogaster. Biochim. Biophys. Acta 1830 (1), 2256–2266.
PetracheVoicu, S.N., Dinu, D., Sima, C., Hermenean, A., Ardelean, A., Codrici, E., Stan, M.S., Zărnescu, O., Dinischiotu, A., 2015. Silica nanoparticles induce oxidative stress and autophagy but not apoptosis in the MRC-5 cell line. Int. J. Mol. Sci. 16 (12), 29398–29416.
Pogribna, M., Hammons, G., 2021. Epigenetic effects of nanomaterials and nanoparticles. J. Nanobiotechnol. 19, 2.

Ramesh, R., Kavitha, P., Kanipandian, N., Arun, S., Thirumurugan, R., Subramanian, P., 2013. Alteration of antioxidant enzymes and impairment of DNA in the SiO2 nanoparticles exposed zebra fish (Danio rerio). Environ. Monit. Assess. 185 (7), 5873–5881.
Reich, S., Weinstein, D.C., 2019. Repression of inappropriate gene expression in the vertebrate embryonic ectoderm. Genes 10, 895.
Reifers, F., Walsh, E.C., Léger, S., Stainier, D.Y., Brand, M., 2000. Induction and differentiation of the zebrafish heart requires fibroblast growth factor 8 (fgf8/acerebellar). Development (Camb. Engl.) 127 (2), 225–235.
Robberecht, H., Van Dyck, K., Bosscher, D., Van Cauwenbergh, R., 2008. Silicon in foods: content and bioavailability. Int. J. Food Prop. 11 (3), 638–645.
Saint-Cricq, P., Deshayes, S., Zink, J.I., Kasko, A.M., 2015. Magnetic field activated drug delivery using thermodegradable azo-functionalised PEG-coated core-shell mesoporous silica nanoparticles. Nanoscale 7 (31), 13168–13172.
Santagati, F., Rijli, F.M., 2003. Cranial neural crest and the building of the vertebrate head. Nat. Rev. Neurosci. 4 (10), 806–818.
Schneider, R.A., Hu, D., Rubenstein, J.L., Maden, M., Helms, J.A., 2001. Local retinoid signaling coordinates forebrain and facial morphogenesis by maintaining FGF8 and SHH. Development 128, 2755–2767.
Session, A.M., Uno, Y., Kwon, T., Chapman, J.A., Toyoda, A., Takahashi, S., Fukui, A., Hikosaka, A., Suzuki, A., Kondo, M., van Heeringen, S.J., Quigley, I., Heinz, S., Ogino, H., Ochi, H., Hellsten, U., Lyons, J.B., Simakov, O., Putnam, N., Stites, J., Rokhsar, D.S., 2016. Genome evolution in the allotetraploid frog Xenopuslaevis. Nature 538 (7625), 336–343.
Shi, Y., Katsev, S., Cai, C., Evans, S., 2000. BMP signaling is required for heart formation in vertebrates. Dev. Biol. 224 (2), 226–237.
Smith, D.M., Nielsen, C., Tabin, C.J., Roberts, D.J., 2000. Roles of BMP signaling and Nkx2.5 in patterning at the chick midgut-foregut boundary. Development (Camb. Engl.) 127 (17), 3671–3681.
Sonin, D.L., Korolev, D.V., Postnov, V.N., Naumysheva, E.B., Pochkaeva, E.I., Vasyutina, M.L., Galagudza, M.M., 2016. Silicon-containing nanocarriers for targeted drug delivery: synthesis, physicochemical properties and acute toxicity. Drug Deliv. 23 (5), 1747–1756.
Spokony, R.F., Aoki, Y., Saint-Germain, N., Magner-Fink, E., Saint-Jeannet, J.P., 2002. The transcription factor Sox9 is required for cranial neural crest development in Xenopus. Development (Camb. Engl.) 129 (2), 421–432.
Stuhlmiller, T.J., García-Castro, M.I., 2012. Current perspectives of the signaling pathways directing neural crest induction. Cell. Mol. Life Sci. 69 (22), 3715–3737.
Sun, L., Li, Y., Liu, X., Jin, M., Zhang, L., Du, Z., Guo, C., Huang, P., Sun, Z., 2011. Cytotoxicity and mitochondrial damage caused by silica nanoparticles. Toxicol. Vitro 25 (8), 1619–1629.
Symens, N., Walczak, R., Demeester, J., Mattaj, I., De Smedt, S.C., Remaut, K., 2011. Nuclear inclusion of nontargeted and chromatin-targeted polystyrene beads and plasmid DNA containing nanoparticles. Mol. Pharm. 8 (5), 1757–1766.
Takagi, C., Sakamaki, K., Morita, H., Hara, Y., Suzuki, M., Kinoshita, N., Ueno, N., 2013. Transgenic Xenopus laevis for live imaging in cell and developmental biology. Dev. Growth Differ. 55 (4), 422–433.
Tandon, P., Conlon, F., Furlow, J.D., Horb, M.E., 2017. Expanding the genetic toolkit in Xenopus: approaches and opportunities for human disease modeling. Dev. Biol. 426 (2), 325–335.
Theveneau, E., Mayor, R., 2012. Neural crest delamination and migration: from epithelium-to-mesenchyme transition to collective cell migration. Dev. Biol. 366 (1), 34–54.
Tomlinson, M.L., Field, R.A., Wheeler, G.N., 2005. Xenopus as a model organism in developmental chemical genetic screens. Mol. Biosyst. 1 (3), 223–228.
Topilko, P., Levi, G., Merlo, G., Mantero, S., Desmarquet, C., Mancardi, G., Charnay, P., 1997. Differential regulation of the zinc finger genes Krox-20 and Krox-24 (Egr-1) suggests antagonistic roles in Schwann cells. J. Neurosci. Res. 50 (5), 702–712.
Tseng, H.T., Shah, R., Jamrich, M., 2004. Function and regulation of FoxF1 during Xenopus gut development. Development 131 (15), 3637–3647.
Tussellino, M., Ronca, R., Carotenuto, R., Pallotta, M.M., Furia, M., Capriglione, T., 2016. Chlorpyrifos exposure affects *fgf8, sox9,* and *bmp4* expression required for cranial neural crest morphogenesis and chondrogenesis in *Xenopuslaevis* embryos. Environ. Mol. Mutagen. 57, 630–640.
Tussellino, M., Ronca, R., Formiggini, F., De Marco, N., Fusco, S., Netti, P.A., Carotenuto, R., 2015. Polystyrene nanoparticles affect Xenopuslaevis development. J. Nano Res. 17 (2), 1–17.
van Kesteren, P.C., Cubadda, F., Bouwmeester, H., van Eijkeren, J.C., Dekkers, S., de Jong, W.H., Oomen, A.G., 2015. Novel insights into the risk assessment of the nanomaterial synthetic amorphous silica, additive E551, in food. Nanotoxicology 9 (4), 442–452.
van Wijk, B., Moorman, A.F.M., van den Hoff, M.J.B., 2007. Role of bone morphogenetic proteins in cardiac differentiation. Cardiovasc. Res. 74 (2), 244–255.
Vranic, S., Shimada, Y., Ichihara, S., Kimata, M., Wu, W., Tanaka, T., Boland, S., Tran, L., Ichihara, G., 2019. Toxicological evaluation of SiO2 nanoparticles by zebrafish embryo toxicity test. Int. J. Mol. Sci. 20 (4), 882.
Xie, G., Sun, J., Zhong, G., Shi, L., Zhang, D., 2010. Biodistribution and toxicity of intravenously administered silica nanoparticles in mice. Arch. Toxicol. 84 (3), 183–190.
Xue, J.Y., Li, X., Sun, M.Z., Wang, Y.P., Wu, M., Zhang, C.Y., Wang, Y.N., Liu, B., Zhang, Y.S., Zhao, X., Feng, X.Z., 2013. An assessment of the impact of SiO2 nanoparticles of different sizes on the rest/wake behavior and the developmental profile of zebrafish larvae. Small 9 (18), 3161–3168.
Yamaguchi, T.P., 2001. Heads or tails: Wnts and anterior-posterior patterning. Curr. Biol. 11 (17), R713–R724.
Yang, H., Liu, C., Yang, D., Zhang, H., Xi, Z., 2009. Comparative study of cytotoxicity, oxidative stress and genotoxicity induced by four typical nanomaterials: the role of particle size, shape and composition. J. Appl. Toxicol. 29, 69–78.
Yi, Wang, Li, Yin, Wang, Aldalbahi, El-Sayed, Wang, Chen, Fan, 2016. Silica nanoparticles target a wnt signal transducer for degradation and impair embryonic development in zebrafish. Theranostics 6 (11), 1810–1820.
Yu, Z., Li, Q., Wang, J., Yu, Y., Wang, Y., Zhou, Q., Li, P., 2020. Reactive oxygen species-related nanoparticle toxicity in the biomedical field. Nanoscale Res.Lett. 15 (1), 115.
Zou, Y., Li, Q., Jiang, L., Guo, C., Li, Y., Yu, Y., Li, Y., Duan, J., Sun, Z., 2016. DNA hypermethylation of CREB3L1 and bcl-2 associated with the mitochondrial-mediated apoptosis via PI3K/akt pathway in human BEAS-2B cells exposure to silica nanoparticles. PLoS One 11 (6), e0158475.